Korean J. Chem. Eng., 33(12), 3417-3424 (2016)
DOI: 10.1007/s11814-016-0206-3

pISSN: 0256-1115
eISSN: 1975-7220

Production of butene and butadiene by oxidative dehydrogenation of butane over carbon nanomaterial catalysts

Sungwon Park, Yehwon Lee, Geonjoong Kim, and Sungwon Hwang†

Chemical Engineering, Inha University, 100 Inha-ro, Nam-gu, Incheon 22212, Korea
(*Received 24 April 2016 • accepted 12 July 2016*)

Abstract−C4 alkenes are generally used to produce synthetic rubbers, plastics, and other important chemicals. Transition metal oxides are traditionally used as catalysts to produce C4 alkenes from n-butane by oxidative dehydrogenation (ODH). On the other hand, metal-free carbon nanomaterials are receiving much attention as catalysts for ODH due to their environmental benignity, corrosion resistance, and unique surface properties. In this work, a systematic methodology was designed to measure conversion of the reactants, selectivity to main products, and other catalytic performances of a set of carbon catalysts, including graphite and activated carbon. The experiments were carried out under a wide range of reaction conditions, and the reaction mechanism and kinetics were developed based on Mars-van Krevelen interpretation of the experimental results.

Keywords: Catalyst, Carbon Material, Oxidative Dehydrogenation, Kinetic, Modeling

INTRODUCTION

C4 alkenes, including butenes and butadiene are generally used to produce synthetic rubbers, plastics, and other important chemicals [1]. The global demand for butene and butadiene has increased significantly in the last few decades, and the process for the production of butene and butadiene has received much attention.

Currently, the naphtha catalytic cracking (NCC) process accounts for almost 90% of total butadiene production in the world. This process has a reaction mechanism of breaking naphtha (C5-C12) into lighter hydrocarbons, such as ethene, propene, butene, and butadiene [2]. However, it has a few operational disadvantages. First, the NCC process produces not only butadiene but also many other petrochemicals, such as ethylene, propylene, and isobutene, requiring an additional separation unit operations. Second, the process consumes high energy owing to the high reaction temperature required for reaction [3]. As a result, the NCC process requires relatively high capital and operating cost [4]. Therefore, increasing research attention is paid to alternative processes, such as direct dehydrogenation of n-butane. Main reaction mechanisms of this process are shown in Eqs. (1) and (2).

$$C_nH_{2n+2} \leftrightarrow C_nH_{2n}+H_2 \quad (1)$$

$$C_nH_{2n+2} \leftrightarrow C_nH_{2n-2}+2H_2 \quad (2)$$

This reaction has been studied as an alternative process for the production of light olefins since the early 1930s [5]. However, a few problems were found to make the direct hydrogenation process commercialized. First, the dehydrogenation reaction is highly endothermic. Therefore, its equilibrium shifts to product formation only under relatively high reaction temperature (e.g., 500 to 650 °C) [6]. Second, when a catalyst is used, high temperature causes the cracking of hydrocarbons and coke formation on the catalyst surface. Coke formation decreases catalytic activity and selectivity for the main product, and requires additional catalyst regeneration steps [7]. Third, the endothermic equilibrium reaction consumes significant energy inside a reactor throughout the reaction to increase conversion ratio. Lastly, the total number of molecules is lower on the reactant side of the equilibrium. Therefore, high pressure is preferred for commercial process to increase conversion ratio [8,9].

Consequently, reactions of butane with oxygen such as the oxidative dehydrogenation (ODH) of n-butane have been considered as alternative to direct dehydrogenation [10].

$$C_nH_{2n+2}+0.5O_2 \leftrightarrow C_nH_{2n}+H_2O \quad (3)$$

$$C_nH_{2n+2}+O_2 \leftrightarrow C_nH_{2n-2}+2H_2O \quad (4)$$

In this reaction, butane reacts with oxygen on the surface of catalyst, producing a C4 olefin. ODH is an exothermic process, and it can be carried out at relatively low temperature (e.g., 300 to 400 °C), thus requiring much less energy consumption than the direct dehydrogenation process [11]. Furthermore, presence of oxygen promotes the combustion of the cokes that are deposited on the catalyst surface, preventing its deactivation. Therefore, ODH has been

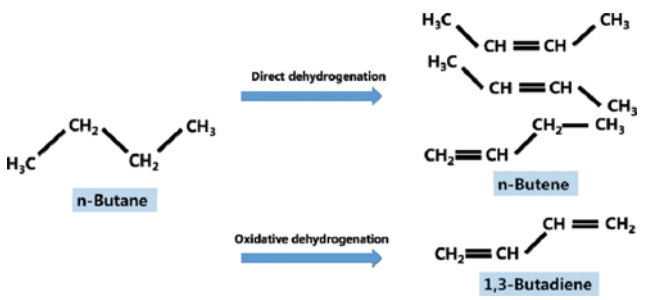

Fig. 1. Direct and oxidative dehydrogenation processes.

†To whom correspondence should be addressed.
E-mail: sungwon.hwang@inha.ac.kr

Table 1. Surface area, particle size and supplier with different carbon materials

Catalyst	Surface area (m^2/g)	Particle size	Supplier
Sigma graphite	600	Less than 150 μm	Sigma aldrich
Expendable graphite	200	250 μm	GRAFGUARD
Timcal graphite	62	45 μm	Timcal
Rod graphite	-	L=150 mm, Diam=6 mm	Sigma aldrich
SA4 activated carbon	1150	34 μm	Cabot norit
Coconut activated carbon	900	4-8 mesh	Han Yan

increasingly recognized as an attractive alternative for the production of butene and butadiene.

Complex metal oxides, such as bismuth molybdates and V/MgO, have been studied as potential catalysts for the ODH of light alkanes to alkenes [12]. However, current ODH catalysts exhibit limited activity and selectivity, resulting from the deep oxidation of the hydrocarbon. Furthermore, promoters are needed to improve the oxygen mobility and performance of these catalysts. Consequently, research has been continuously conducted to find novel catalysts for ODH [13].

It has been recently reported that the quinone/hydroquinone groups in a black carbonaceous material called "active coke" are catalytically active for ODH. The reaction of active coke with oxygen at high temperature leads to the formation of functional groups such as carbonyl, quinone, and hydroquinone groups that are regarded as the active sites [14].

This result promoted an increase of research attention to carbon-based materials as a catalyst for ODH [15].

Carbon materials as catalysts have attracted increasing interest because of their unique surface chemistry, porosity, specific characteristics, and relatively low impact on environmental damage. The ketone and quinone groups on the surface of carbon materials are rich in electrons, meaning that they have high potential to promote redox reactions. Hydrogen atoms in the C-H bonds of alkanes are attracted to the Lewis basic sites on the surface of the carbon. Gas phase oxygen then reacts with the abstracted hydrogen, and the active site is regenerated with the simultaneous formation of water [16].

Despite the large number of literature studies dealing with the ODH of alkanes to alkenes over carbon catalysts, a detailed study of the kinetics and mechanisms of the process has not been presented. Thus, in this work, different carbon materials, including sigma graphite, expendable graphite, timcal graphite, rod graphite, SA4 activated carbon, and activated coconut carbon, were investigated as catalysts for the ODH of butane to butene and butadiene. In addition, a set of kinetic models for the ODH of butane over carbon catalysts has been developed and incorporated into the reaction model. Lastly, the accuracy of the model was tested by comparing the simulation results with the experimental data. In particular, this article illustrates different mathematical techniques for the design of a complex reaction system over novel catalysts.

EXPERIMENTAL SETTING

Sigma graphite, expendable graphite, timcal graphite, rod graphite, SA4 activated carbon, and activated coconut carbon were used as catalysts without further purification. In Table 1, the surface, particle size and supplier with different carbon materials are summarized.

The catalytic tests were performed at 450-550 °C under atmospheric pressure in a continuous-flow fixed-bed reactor at a total flow rate of 70 mL/min. The reactor was prepared in a stainless steel with a tube I.D. of 10 mm and length of 10 cm. The reactor was placed inside an electrical furnace, and a K type thermocouple was installed in the center of the catalyst bed to monitor the reaction temperature.

The flow rates of air, butane, and nitrogen were adjusted by a Brooks mass flow controller. All lines were heated to avoid condensation in the system. For each run, 150 mg catalyst was used, and the reactant mixture of n-butane and O_2 in a ratio of 1 : 2 was used with N_2 as inert material. Carbon catalysts were placed inside the reactor as a fine powder; thus it was assumed that no internal diffusion occurred inside the reactor. In addition, external mass transfer resistance was considered to be negligible. Therefore, the reaction inside the reactor was assumed to be isothermal.

Gas mixtures were analyzed by on-line gas chromatography (GC; Hewlett-Packard, HP-6890) using flame ionization detection (FID). Nitrogen was used as carrier gas, and temperature of the column was maintained at 50 °C. Furthermore, the following experiment setting was used to test catalysts:

- Mass of catalyst: 150 mg

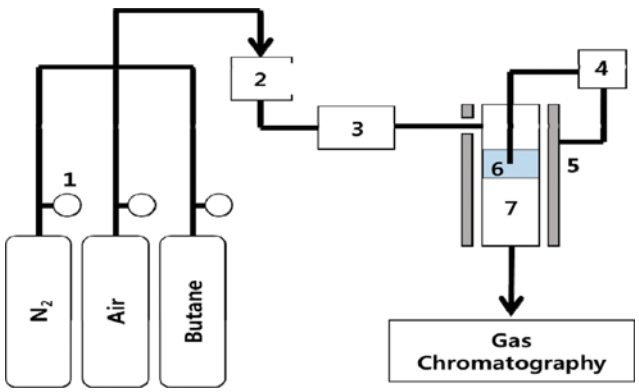

Fig. 2. Schematic diagram of the continuous flow reactor system.

1. Pressure regulator
2. Gas mixer
3. Preheater
4. Temperature controller
5. Furnace
6. Catalyst
7. Reactor

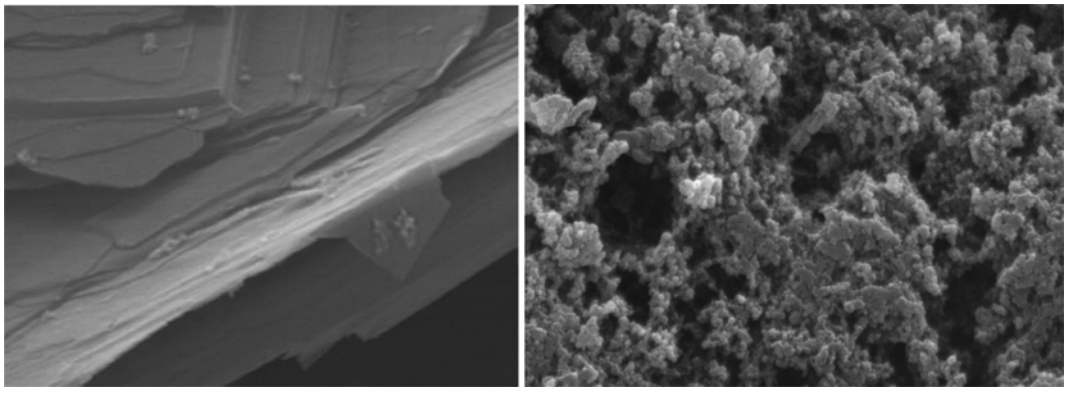

Fig. 3. SEM images of graphite and activated carbon.

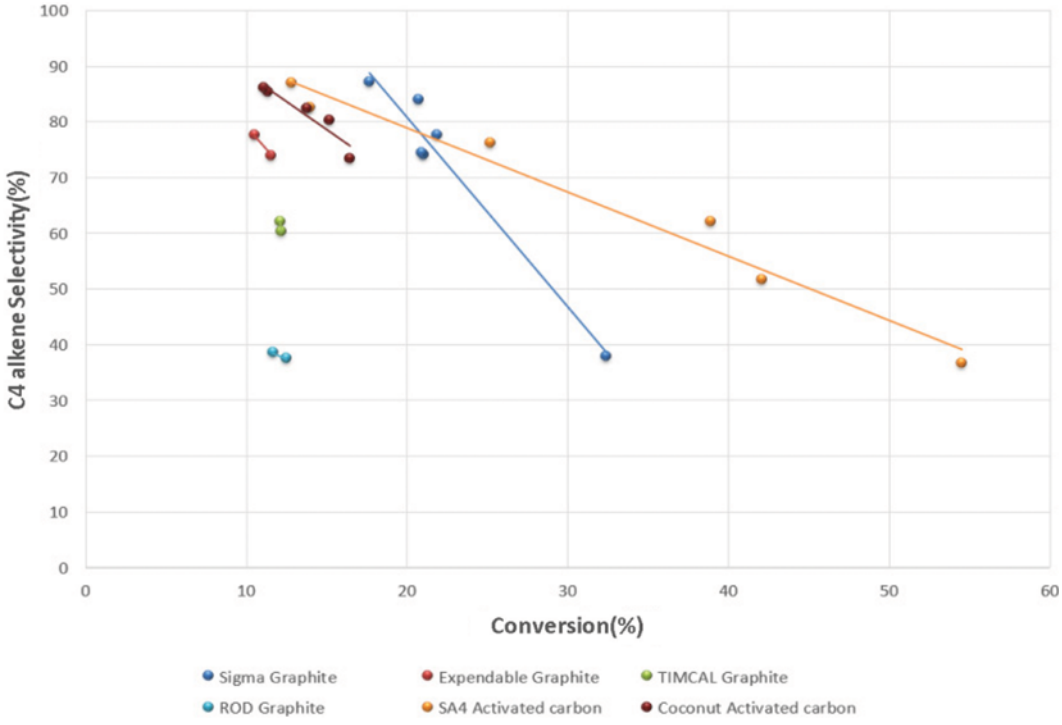

Fig. 4. Conversion vs. selectivity for the different carbon catalysts.

- Time on stream: 2 h
- Butane flow rate: 1.5 mL/min
- Oxygen flow rate: 3 mL/min

The performance of the catalyst was calculated in terms of the following equations:

$$C_4H_{10}\ \text{Conversion}\ (\%) = \frac{C_4H_{10}(\text{Input}) - C_4H_{10}(\text{Ouput})}{C_4H_{10}(\text{Input})} \quad (5)$$

$$C_XH_Y\ \text{Selectivity}\ (\%) = \frac{C_XH_Y(\text{Product})}{\text{Hydrocarbon(Products)}} \quad (6)$$

A schematic diagram of the unit to produce the kinetic data is shown in Fig. 2. The carbon samples were analyzed by scanning electron microscopy (SEM), and the images are shown in Fig. 3. The graphite has a flaked morphology with an average size of 45 μm, while the activated carbon presents a highly porous structure.

EXPERIMENTAL RESULTS

1. Results and Discussion

Fig. 4 shows the relationship between conversion and selectivity to produce C4 olefins through ODH of butane over different catalysts. Selectivity for the production of C4 olefins decreases as conversion increases. At the same conversion of butane, SA4 activated carbon and sigma graphite show higher selectivity for C4 olefins than the other catalysts.

Details of the product distributions obtained over SA4 activated carbon and sigma graphite catalysts are given in Fig. 5. For the same conversion (i.e., 25%) of butane, a higher selectivity for C4 butene is exhibited by the SA4 activated carbon, while a higher

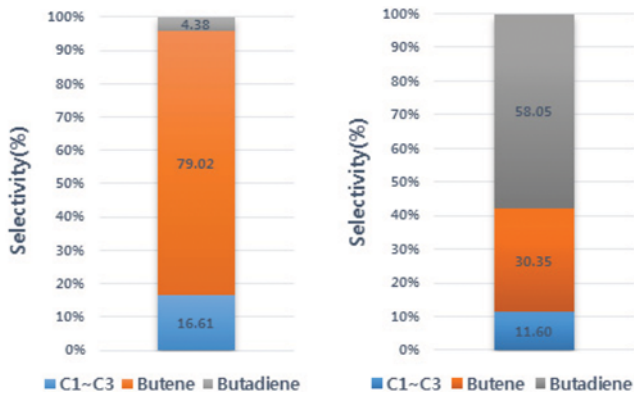

Fig. 5. Selectivity results obtained over SA4 activated carbon (left) and sigma graphite (right).

selectivity for butadiene is exhibited by the sigma graphite. However, the selectivity for C4 olefins over the sigma graphite significantly decreases as conversion increases. The reason for this is assumed to be that the butadiene that has two double bonds tends to be oxidized more readily to by-products, compared with butane and butene.

Thus, the SA4 catalyst shows the highest selectivity for the production of C4 alkenes overall.

2. Reaction Network

The effect of reaction conditions cannot be quantified without a comprehensive understanding of the reaction network and kinetics. For the purpose of identifying the reaction network and each reaction kinetic, the following facts were ascertained from the experimental results: (i) The mole fractions of the butadiene and butene pass through a maximum point; (ii) measurable amounts of butadiene and butene are produced at low conversion of the butane; and (iii) the mole fraction of the side products (C1-C3) increases linearly with residence time.

On the basis of (i) and (ii), butene and butadiene are assumed to be primary intermediate products. Furthermore, we concluded that the reactions of C1-C3 species could be ignored, based on item (iii) above.

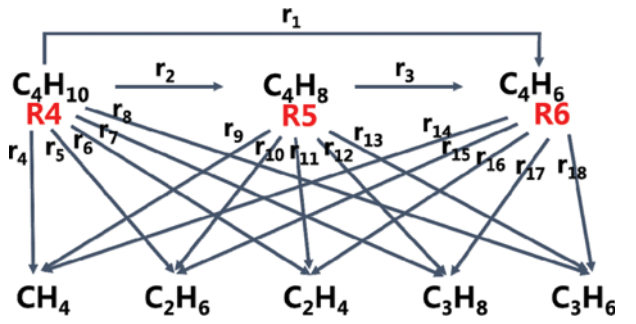

Fig. 6. Superstructure network for the possible reactions.

Based on experimental results and theoretical study, a detailed superstructure network is proposed, as shown in Fig. 6. The reaction network includes both series and parallel networks, where butene is formed only from butane; butadiene is formed from both butane and butene; and C1-C3 hydrocarbons (i.e., methane, ethane, ethene, propane, and propene) are formed from all the C4 hydrocarbons (i.e., butane, butene, and butadiene). Reactions R4, R5, and R6 in this scheme refer to the formation of methane, ethane, ethene, propane, and propene from butane, butene, and butadiene, respectively.

The stoichiometric equations corresponding to main reactions, r_1 to r_3, are given as follows:

$$C_4H_{10}+0.5O_2 \rightarrow C_4H_8+H_2O \quad (7)$$

Table 2. Super structure of the possible reactions

	r_1	r_2	r_3	R_4	R_5	R_6
Model 1	1	1	1	1	0	0
Model 2	1	1	1	1	1	0
Model 3	1	1	1	1	1	1
Model 4	1	1	1	0	1	1
Model 5	1	1	1	0	1	0
Model 6	1	1	1	0	0	1
Model 7	1	1	1	1	0	1

Table 3. Results of the oxidative dehydrogenation reaction over SA4 activated carbon

Residence time (h)	Mole fraction (-)								Yield (%)	
	Butane	Butene	Butadiene	Methane	Ethane	Ethene	Propane	Propene	Butene	Butadiene
0.00000	1.0000	0.0000	0.0000	0.0000	0.0000	0.0000	0.0000	0.0000	0.0000	0.0000
0.00041	0.8031	0.1322	0.0280	0.0041	0.0033	0.0065	0.0035	0.0091	13.2200	2.8000
0.00047	0.7839	0.1421	0.0320	0.0052	0.0041	0.0076	0.0038	0.0106	14.2100	3.2000
0.00054	0.7533	0.1591	0.0350	0.0072	0.0058	0.0093	0.0045	0.0136	15.9100	3.5000
0.00065	0.7002	0.1900	0.0370	0.0119	0.0097	0.0134	0.0061	0.0202	19.0000	3.7000
0.00082	0.6133	0.2300	0.0388	0.0211	0.0160	0.0174	0.0096	0.0314	23.0000	3.8800
0.00093	0.5837	0.2647	0.0412	0.0253	0.0190	0.0191	0.0112	0.0357	26.4700	4.1200
0.00109	0.5493	0.2775	0.0432	0.0307	0.0232	0.0212	0.0139	0.0409	27.7500	4.3200
0.00131	0.5061	0.2892	0.0461	0.0390	0.0296	0.0241	0.0177	0.0482	28.9200	4.6100
0.00163	0.4491	0.2976	0.0496	0.0527	0.0403	0.0282	0.0239	0.0586	29.7600	4.9600
0.00218	0.3802	0.2959	0.0541	0.0748	0.0569	0.0335	0.0321	0.0722	29.5900	5.4100
0.00327	0.3117	0.2751	0.0538	0.1095	0.0803	0.0395	0.0419	0.0862	27.5100	5.3800

$$C_4H_8+0.5O_2\rightarrow C_4H_6+H_2O \quad (8)$$

$$C_4H_{10}+O_2\rightarrow C_4H_6+2H_2O \quad (9)$$

2-1. Rival Models

For a complex reaction system, a number of feasible reaction schemes can be considered. In such cases, it may be inappropriate to fit kinetic parameters to all potential reactions simultaneously as it would require considerable computational time and effort. Therefore, we used seven standard models to represent the ODH reaction kinetics over SA4 activated carbon at a reaction temperature of 500 °C and residence times in the range of 0.00041-0.00327 h. Table 3 shows the results of the experiments along with residence times. The difference between each model is shown in Table 2. The numbers 1 and 0 indicate that the reaction occurs or does not occur, respectively.

3. The Kinetic Model

Appropriate modeling of the catalytic reaction kinetics is essential to develop successful mathematical modeling of the ODH process. It has been reported that carbonyl/quinone groups on the catalyst surface play an important role as the active sites for the reaction [14]. Therefore, Mars-van Krevelen redox mechanisms were used, in which the quinone groups are reduced to hydroquinones by the adsorbed butane and reoxidized to quinone by gaseous oxygen [17].

The Mars-van Krevelen model is also often used to rationalize partial oxidation reactions over conventional metal oxides [18]:

$$r=\frac{1}{\left(\frac{1}{k_O P_{O_2}^n}\right)+\left(\frac{1}{k_r P_R}\right)} \quad (10)$$

where, r (mol/h·g) is the reaction rate, n is the order of the partial pressure of oxygen, P_{O_2} (atm) is the partial pressure of the oxygen, P_R (atm) is the partial pressure of the hydrocarbon, k_o (mol/h·g·atm) is the oxidation rate constant, and k_r (mol/h·g·atm) is the reduction rate constant. If we assume that the oxidation rate constant is much larger than the reduction rate constant, the expression can be simplified as:

$$r=k_r P_R \quad (11)$$

Using this expression, a kinetic model was fitted to the experimental data, which was obtained under wide range of residence times.

4. Parameter Identification

Parameter identification in the study of reaction kinetics can be regarded as an optimization problem. The objective is to minimize the difference between the measured and predicted values. Eleven sets of data were used to fit the parameters of reaction kinetics. Each experimental data set was obtained after 2 h on stream, when the system exhibited steady state conditions. In the optimization formula, an objective function, F, is expressed in the form of Eq. (12) to minimize the overall difference between the predicted values from the model and the experimental data at each measured point.

$$F=\Sigma_{i=1}^{n}\Sigma_{j=1}^{N}(y_{expi}-y_{cali})^2 \quad (12)$$

where, the $y_{exp\,i}$ and $y_{cal\,i}$ are the experimental and calculated values of species i, n is the number of species, and N is the number of data points.

4. Genetic Algorithm

A genetic algorithm (GA) was used to minimize the objective function, F. A genetic algorithm is a commonly used optimization algorithm to solve both constrained and unconstrained problems based on a natural selection process. The GA repeatedly amends the population of each solution from the present population and uses them as the parents to produce children for the next generation. Over consecutive generations, the population reaches the optimal solution. Unlike other algorithms that generate a single point at each iteration, the GA generates a population of multiple points at each iteration. Furthermore, mutation of the GA allows the algorithm to avoid reaching the local minimum point by preventing the populations from becoming too similar. The performance of the GA depends on different parameters, such as generation number, population size, crossover, and mutation. The GA parameters used in this study are presented in Table 4.

5. Evaluation of Rival Models

5-1. Paired T-test

Selection of the model that most closely matches the experimental data among many candidates is quite important. For this, the paired t-test, which is a statistical technique used to compare the mean of two groups, was employed to verify the accuracy of the predicted values for the experimental values. Typically, a constraint is considered to be statistically significant if p is less than 0.05. In Table 5, the result of the paired t-test for each model is shown. If h is equal to 0, the experimental data and predicted value

Table 4. GA Parameter values used in the present study

GA Parameter	Value
Generations	200
Population size	100
Crossover probability	0.8
Mutation probability	0.2

Table 5. Result of the paired t-test for each model

		Butane	Butene	Butadiene	Standard error (F)
Model 1	h	1	0	0	0.0538
	p	0.015	0.109	0.175	
Model 2	h	0	0	0	0.0408
	p	0.387	0.942	0.227	
Model 3	h	0	0	0	0.0337
	p	0.292	0.775	0.897	
Model 4	h	0	0	0	0.0420
	p	0.253	0.289	0.217	
Model 5	h	0	1	0	0.0438
	p	0.468	0.001	0.318	
Model 6	h	0	0	1	0.0665
	p	0.429	0.444	0.002	
Model 7	h	0	0	0	0.0338
	p	0.275	0.630	0.997	

can be considered to be equal. However, if h is equal to 1, there is significant difference between the two values.

As we can see from Table 5, models 1, 5, and 6 do not properly represent the experimental values for butane, butene, and butadiene. However, models 2, 3, 4, and 7 afford predicted values that are in good agreement with the experimental results.

5-2. Covariance/Correlation Matrix

Covariance/correlation analysis was used to determine the relationships between the parameters that were fitted in the model. Covariance is a measurement of how much two variables change together. In the covariance matrix, the element in the i, j position represents the covariance between the i and j elements of a vector. Covariance can be calculated from the following formula:

$$\mathrm{Cov}[X, Y] = E\begin{bmatrix} (X_1-E[X_1])(Y_1-E[Y_1]) & \cdots & (X_1-E[X_1])(Y_j-E[Y_j]) \\ \vdots & \ddots & \vdots \\ (X_i-E[X_i])(Y_1-E[Y_1]) & \cdots & (X_i-E[X_i])(Y_j-E[Y_j]) \end{bmatrix} \quad (13)$$

$$= \begin{bmatrix} E(X_1-E[X_1])(Y_1-E[Y_1]) & \cdots & E(X_1-E[X_1])(Y_j-E[Y_j]) \\ \vdots & \ddots & \vdots \\ E(X_i-E[X_i])(Y_1-E[Y_1]) & \cdots & E(X_i-E[X_i])(Y_j-E[Y_j]) \end{bmatrix} \quad (14)$$

$$= E\begin{bmatrix} \mathrm{Cov}[X_1, Y_1] & \cdots & \mathrm{Cov}[X_1, Y_j] \\ \vdots & \ddots & \vdots \\ \mathrm{Cov}[X_i, Y_1] & \cdots & \mathrm{Cov}[X_i, Y_j] \end{bmatrix} \quad (15)$$

where, E is the mean, X_i is the score in each of the i data sets, and Cov is a covariance matrix.

The main diagonal of the covariance matrix contains the variances of the parameter estimates, while the off-diagonal elements characterize the covariance between pairs of parameters, which is a measure of the dependence between the parameters. To normalize the significance of the relationship, the correlation can be used. The correlation matrix of the parameters can be calculated from the covariance matrix:

$$\mathrm{Cor}[X, Y] = \frac{\mathrm{Cov}[X, Y]}{\mathrm{sd}[X] * \mathrm{sd}[Y]} \quad (16)$$

where, sd[X] and sd[Y] are the standard deviations of X and Y, respectively.

Each off-diagonal element of the correlation matrix is between 1 and −1. When the sign is positive, the variables are defined as positively correlated; when the sign is negative, the variables are defined as negatively correlated; and when the sign is 0, the vari-

Table 6. Result of correlation matrix for model 6

Correlation matrix (model 6)								
Parameters	k1	k2	k3	k14	k15	k16	k17	k18
k1	1							
k2	0.034	1						
k3	−0.101	−0.010	1					
k14	−0.036	0.130	0.000	1				
k15	0.113	−0.135	−0.130	0.223	1			
k16	0.111	0.249	0.118	0.040	−0.035	1		
k17	−0.024	0.007	−0.015	0.122	0.173	−0.242	1	
k18	0.144	0.000	0.129	−0.066	0.174	0.047	−0.081	1

Table 7. Result of correlation matrix for model 7

Correlation matrix (model 7)													
Parameters	k1	k2	k3	k4	k5	k6	k7	k8	k14	k15	k16	k17	k18
k1	1												
k2	0.280	1											
k3	0.076	0.023	1										
k4	0.134	−0.171	0.256	1									
k5	0.183	0.243	0.058	0.211	1								
k6	−0.138	0.036	−0.012	0.031	0.158	1							
k7	0.163	0.341	−0.072	0.099	0.255	−0.180	1						
k8	0.041	0.305	−0.051	−0.131	0.152	0.068	−0.012	1					
k14	−0.008	−0.007	0.062	0.155	0.239	0.027	0.176	−0.036	1				
k15	0.056	−0.018	0.063	0.123	−0.071	−0.060	0.015	−0.059	0.073	1			
k16	−0.052	−0.341	−0.236	0.079	0.163	0.049	0.072	−0.323	0.154	−0.026	1		
k17	0.156	0.090	0.035	0.063	0.207	−0.079	0.149	0.055	0.122	0.237	0.069	1	
k18	0.168	0.041	−0.094	−0.031	0.008	0.146	−0.185	0.001	−0.053	0.117	−0.048	0.086	1

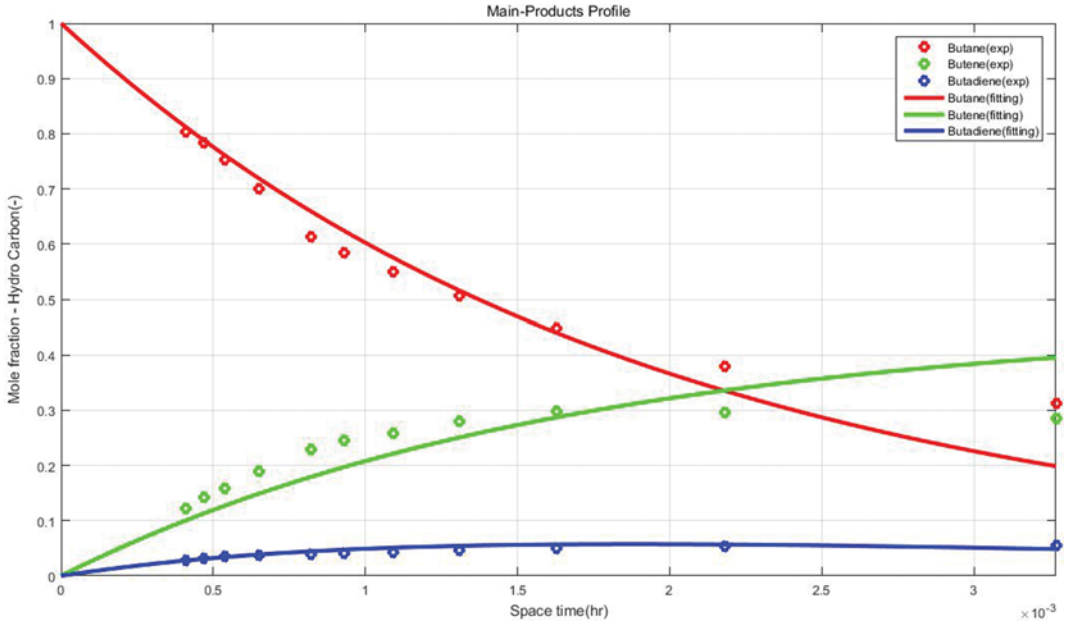

Fig. 7. Prediction of mole fractions: Main products profile.

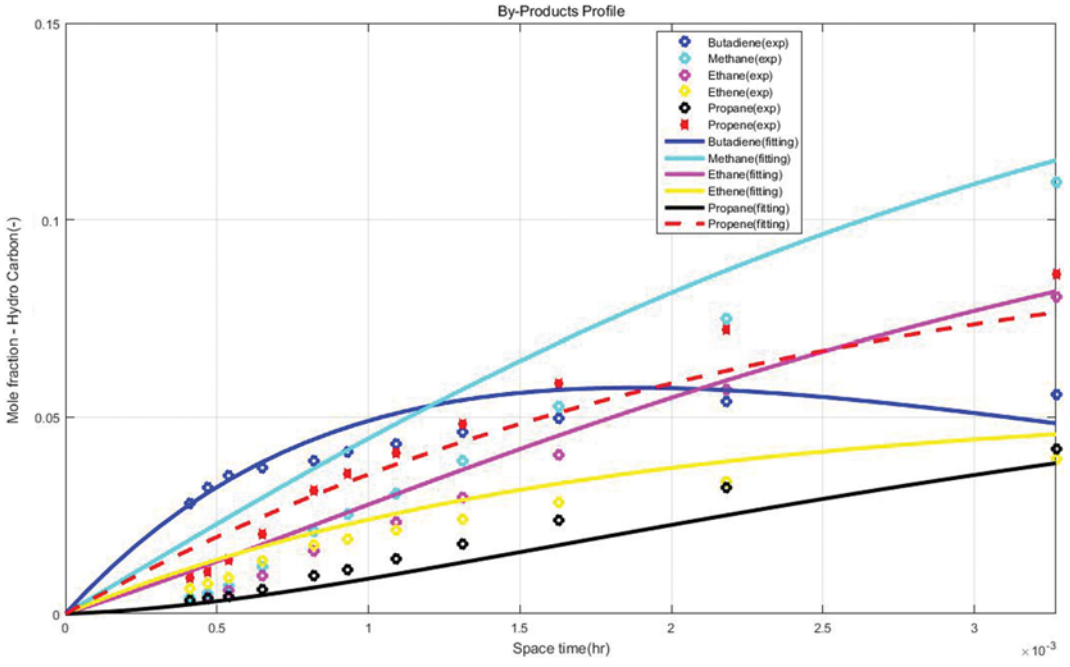

Fig. 8. Prediction of mole fractions: By-products profile.

ables are defined as uncorrelated. As the absolute values approach 1, the parameters become more correlated and the parameter estimation becomes poorer. However, as the absolute value approaches 0, the parameter becomes more independent, and the parameter estimation has higher accuracy. In an ideal reaction process, each reaction takes place independently, so that the correlation of the parameters of each reaction should be 0 [19]. High correlation between parameters may occur for several reasons, such as an inappropriate model and/or bad experimental design [20].

The correlation matrix results shown in Tables 6 and 7 show that, in models 6 and 7, all parameters exhibit very low correlation between each other in. But, the parameters in the other models (i.e., models 1, 2, 3, 4, and 5) exhibit a strong correlation.

Model 7, which represents the experimental data with high accuracy and exhibits the smallest correlation between the parameters, was selected as the most appropriate model. Figs. 7 and 8 illustrate how the developed model 7 is able to predict change of each component along various residence times at a reaction temperature of 500 °C and a feed component ratio of butane to O2 of 1 : 2. The calculated kinetic parameters are shown in Table 8.

Table 8. Calculated kinetic parameters from model 7

Parameter (mol/h·g·atm)	Model 7
k1	175.018
k2	37.042
k3	52.729
k4	0.017
k5	2.989
k6	6.026
k7	0.121
k8	32.025
k14	0.032
k15	115.428
k16	7.791
k17	130.062
k18	206.185

CONCLUSION

The production of butene and butadiene by ODH over Sigma graphite, expandable graphite, timcal graphite, rod graphite, SA4 activated carbon, and activated coconut carbon was studied. These carbon catalysts exhibited relatively stable catalytic performance over a long operating time. The selectivity for C4 olefins in the product was found to decrease as the conversion ratio increased, whereas the C1-C3 content in the product increased as the conversion increased. Sigma graphite and SA4 activated carbon showed the highest selectivity for C4 olefins. Sigma graphite showed superior selectivity for the production of butadiene, while SA4 activated carbon showed high selectivity for butene. However, selectivity for the production of C4 olefins over Sigma graphite decreased sharply with increased conversion ratio because of the relatively high reactivity of the two double bonds. Further kinetic study was performed on the ODH over SA4 activated carbon, as it showed the highest selectivity for C4 olefins under a wide range of conversion ratios.

The Mars-van Krevelen mechanism was assumed to investigate the reaction kinetics. GA algorithms, paired t-test results, and a covariance/correlation matrix were employed to determine the most appropriate reaction pathway and the rate constant of each reaction. Model 7, in which C1-C3 hydrocarbon was produced from butane and butadiene, was confirmed to be the most appropriate model. The model adequately fitted the data that was obtained under various residence time, and the respective kinetic parameters were obtained. In this model, synthesized butadiene was considered to decompose by consecutive reaction due to the active double bonds, which contribute to the decrease of the C4 olefin's yield. Therefore, to obtain maximum yields of olefin, optimization of catalyst amounts inside a bed would be needed.

The proposed methodology is a very efficient, fast, and accurate to identify the rate constants and pathways of complex reactions.

ACKNOWLEDGEMENTS

This research was supported by an INHA UNIVERSITY Research Grant (No. 52728-01).

REFERENCES

1. E. V. Makshina, M. Dusselier, W. Janssens, J. Degreve, P. A. Jacobs and B. F. Sels, *Chem. Soc. Rev.*, **43**, 7917 (2014).
2. Y. Yoshimura, N. Kijima, T. Hayakawa, K. Murata, K. Suzuki, F. Mizukami and T. Shiojima, *Catal. Surveys from Japan*, **4**, 157 (2001).
3. E. Worrell, L. Price, M. Neelis, C. Galitsky and N. Zhou, *World best practice energy intensity values for selected industrial sectors*, Lawrence Berkeley National Laboratory (2007).
4. H. Lim, J. Choi, M. Realff, J. H. Lee and S. Park, *Ind. Eng. Chem. Res.*, **45**, 5738 (2006).
5. D. H. James and W. M. Castor, Styrene, Ullmann's Encyclopedia of Industrial Chemistry (1994).
6. M. M. Bhasin, J. H. McCain, B. V. Vora, T. Imai and P. R. Pujado, *Appl. Catal. A: Gen.*, **221**, 397 (2001).
7. J. Gascón, C. Téllez, J. Herguido and M. Menéndez, *Appl. Catal. A: Gen.*, **248**, 105 (2003).
8. M. Setnička, P. Čičmanec, E. Tvarůžková and R. Bulanek, *Topics in Catalysis*, **56**, 662 (2013).
9. H. Weyten, K. Keizer, A. Kinoo, J. Luyten and R. Leysen, *AIChE J.*, **43**, 1819 (1997).
10. P. A. Batist, J. F. H. Bouwens, G. C. A. Schuit, J. F. H. Bouwens and G. C. A. Schuit, *J. Catal.*, **25**, 1 (1972).
11. S. Vajda, M. J. Pellin, J. P. Greeley, C. L. Marshall, L. A. Curtiss, G. A. Ballentine and P. Zapol, *Nature Mater.*, **8**, 213 (2009).
12. P. A. Batist, A. H. W. M. Der Kinderen, Y. Leeuwenburgh, F. A. Metz and G. C. A. Schuit, *J. Catal.*, **12**, 45 (1968).
13. J. H. Park, H. Noh, J. W. Park, K. Row, K. D. Jung and C. H. Shin, *Appl. Catal. A: Gen.*, **431**, 137 (2012).
14. A. Schraut, G. Emig and H.-G. Sockel, *Appl. Catal.*, **29**, 311 (1987).
15. J. Zhang, X. Liu, R. Blume, A. Zhang, R. Schlögl and D. S. Su, *Science*, **322**, 73 (2008).
16. M. F. R. Pereira, J. L. Figueiredo, J. J. Órfão, P. Serp, P. Kalck and Y. Kihn, *Carbon*, **42**, 2807 (2004).
17. M. F. R. Pereira, J. J. M. Orfao and J. L. Figueiredo, *Appl. Catal. A: Gen.*, **196**, 43 (2000).
18. P. Mars and D. W. Van Krevelen, *Chem. Eng. Sci.*, **3**, 41 (1954).
19. C. N. Yang, *Reviews of Modern Physics*, **34**, 694 (1962).
20. M. Schwaab and J. C. Pinto, *Chem. Eng. Sci.*, **62**, 2750 (2007).